Steady state stability features of the electron–positron plasma diode in a mode with particle reflection from potential extrema

L. A. Bakaleinikov ✉ 📧 ; V. I. Kuznetsov 📧 ; E. Yu. Flegontova 📧 ; D. P. Barsukov 📧 ; I. K. Morozov 📧

Check for updates

View Online

Export Citation

Articles You May Be Interested In

Steady state stability features of the electron–positron plasma diode in a mode with particle reflection from potential extrema

View Online   Export Citation   CrossMark

L. A. Bakaleinikov,[a)] (iD) V. I. Kuznetsov, (iD) E. Yu. Flegontova, (iD) D. P. Barsukov, (iD) and I. K. Morozov (iD)

AFFILIATIONS

Ioffe Institute, St. Petersburg 194021, Russia

[a)]Author to whom correspondence should be addressed: bakal.ammp@mail.ioffe.ru

ABSTRACT

Steady state stability features of a diode with electrons and positrons entering from opposite boundaries and moving without collisions in plasma are numerically studied. The most complex regime when charged particles are reflected from potential barriers is considered. This problem arises, in particular, when modeling pulsar diodes. A small perturbation evolution is studied. It has been established that at the initial stage of the process the perturbation amplitude changes in time according to an exponential law. It is shown that stationary solutions with a potential barrier for electrons located near the electron-emitting electrode and a potential barrier for positrons located near the opposite electrode are stable when the inter-electrode distance is below a certain threshold. As the inter-electrode distance increases, the solutions become unstable. Solutions of another type when barriers reflecting particles are located in the opposite to the emitting electrode parts of the gap are also studied. However, these solutions turned out to be unstable.

I. INTRODUCTION

Plasma consisting of electrons and positrons occurs in various high-energy astrophysical objects, such as neutron stars and their surroundings, black holes and active galactic nuclei, and relativistic jets that produce gamma-ray bursts. In an attempt to better understand its properties, not only much theoretical work is published, but laboratory experiments also have been carried out (see, e.g., the review[1]). One of the most complex astrophysical objects containing electron–positron plasma is pulsars. These radio sources were discovered more than 50 years ago. Despite the fact that the main models describing the structure of the pulsar magnetosphere and the processes occurring in it appeared right after their discovery, there is still no clear idea of either this radiation mechanism or the reason for switching between modes (see, e.g., Ref. 2).

Reference 3 suggests a hypothesis in which the pulsar radiation is caused by electric field oscillations in the diode plasma, arising due to the instability of steady state. This kind of instability is typical for diodes with collisionless plasma, and the mechanism of instability development is the same as that of the well-known Pierce instability, where an electron beam moves in the diode space through an immovable ion background.[4] It should be noted that collective effects in electron–positron plasma created by a laser beam were studied, for example, in Ref. 5.

In Ref. 3, a model of a vacuum diode with counter flows of electrons and positrons entering from opposite boundaries is proposed. Steady states of such diodes are studied in detail in Ref. 6. It has been established that they can be divided into two main types depending on the charged particle movement type: (1) all particles reach the opposite electrode and (2) a particle portion is reflected from the potential barrier within the diode and returns to the emitting electrode. In Ref. 3, an equation for the electric field perturbation for stationary solutions of the first type is derived. For a uniform field distribution, an analytical solution to this equation is found, a dispersion equation is obtained, and dispersion branches are constructed. It has been proven that homogeneous solutions are stable when inter-electrode gap values are less than $\sqrt{2}\,\pi\,\lambda_D$, where λ_D is the Debye–Hückel length. The stability features of the first type state with a nonuniform field distribution were studied in Ref. 7. It is proven that all such solutions are unstable with respect to small perturbations.

In this work, we study numerically the stability features of stationary solutions for the regime with particle reflection from potential barriers. A numerical research method is used due to the fact that to

16 October 2024 11:49:50

date no equation for the electric field perturbation for such a regime has been obtained. The study comes down to calculating the initial stage of a small disturbance development. From the time characteristics of the process, the perturbation eigenmodes are determined, and by the sign of the growth rate, i.e., the real part of the complex frequency, it is determined whether the stationary solution is stable. To validate the results obtained, calculations are carried out using two numerical codes: EK-code and PIC-code.

II. STATIONARY SOLUTIONS

In Refs. 3 and 7, we have obtained an analytical solution of equation for the electric field perturbation. We could use monokinetic velocity distribution functions (VDF) to describe the behavior of charged particles in the cases under consideration. However, in this paper, the stability problem is solved numerically, and it is necessary to use a non-monokinetic VDF. We consider that the non-relativistic electron flow enters from the left electrode, and the positron one enters from the right electrode with VDF slightly different from the monoenergetic one. We assume that the average velocities of incoming particles are the same, but of the opposite sign: $\bar{v}_{p,0} = -\bar{v}_{e,0}$. In this case, the average energies of incoming particles are equal to $W_0 \equiv m_e \bar{v}_{e,0}^2/2 = m_p \bar{v}_{p,0}^2/2$, where m_e and m_p are the electron and positron masses, respectively ($m_e = m_p = m$). We also assume that the particle densities at the electrodes are equal: $n_e = n_p = n_0$. Particles move in the inter-electrode gap without collisions. In addition, we consider that a particle that reaches any electrode is absorbed by it. The potential difference U between the electrodes is assumed to be zero.

We pass on to dimensionless quantities, choosing the particle energy W_0 and the Debye–Hückel length $\lambda_D = [(2\tilde{\varepsilon}_0 W_0)/(e^2 n_{e,0})]^{1/2}$ (e is the electron charge, and $\tilde{\varepsilon}_0$ is the vacuum permittivity) as units of energy and length. For dimensionless coordinate, potential and electric field strength, velocity, and time, we have $\zeta = z/\lambda_D$, $\eta = e\Phi/(2W_0)$, $\varepsilon = eE\lambda_D/(2W_0)$, $u = v/\bar{v}_{e,0}$, and $\tau = t/(\lambda_D/\bar{v}_{e,0})$.

To study processes in the diode collisionless plasma in both stationary and nonstationary modes, it is necessary to solve a system including kinetic equations for charged particles and the Poisson equation, in the right side of which the concentrations of charged particles calculated from the VDF are substituted. The use of a kinetic description is due to the fact that the particles' motion in the interelectrode gap is not single-flow. This system must be completed with boundary conditions for the particle VDFs and PD. We represent the VDF of particles leaving the electrodes in the form of "gates" of small width: $\Delta \ll 1$. In dimensionless variables, it is as follows:

$$f_0^{(e)}(u) = \begin{cases} (2\Delta)^{-1}, & u \in [1-\Delta, 1+\Delta], \\ 0, & u \in (0, 1-\Delta) \cup (1+\Delta, \infty), \end{cases} \quad (1)$$

$$f_0^{(p)}(u) = \begin{cases} (2\Delta)^{-1}, & u \in [-1-\Delta, -1+\Delta], \\ 0, & u \in (-\infty, -1-\Delta) \cup (-1+\Delta, 0). \end{cases} \quad (2)$$

These, in fact, are the boundary conditions for the VDFs. Boundary conditions for the PD are set at different electrodes:

$$\eta(0) = 0, \quad \eta(\delta) = V. \quad (3)$$

At first, we obtain stationary solutions for the VDFs (1) and (2). If Δ is small, they should not differ much from the solutions

corresponding to the case of δ-shaped VDF of particles, described in detail in Ref. 6.

Steady-state PDs are found by solving the second order equation

$$\frac{d^2\eta}{d\zeta^2} = n_e(\eta, \eta_m) - n_p(\eta, \eta_M) \quad (4)$$

(where η_m and η_M are the minimum and maximum potential values that are reflection points for charged particles), which is obtained by substituting expressions for electron n_e and positron n_p densities into the Poisson equation. Formulas for these densities are given by Eqs. (5) and (6). The methods for solving the problems (3) and (4) are presented below.

Steady-state solutions are determined by three dimensionless parameters: the inter-electrode distance $\delta = d/\lambda_D$, the potential difference between the electrodes $V = eU/(2W_0)$, and the electric field strength at the left electrode ε_0. However, they are also slightly influenced by the velocity spread Δ.

For a fixed potential value V, it is convenient to represent steady-state solutions by points on the (ε_0, δ) plane. These points form separate curves, which are called solution branches.[6] They correspond to wave-like potential distributions (PD), which for solutions belonging to different branches differ in the number of extrema and their positions relative to each other. The relation between the potential minimum and maximum η_m and η_M is given by the formula $\eta_M = V - \eta_m$.[6]

In the case of our interest, when $V = 0$ and particles enter the plasma from opposite electrodes with identical charges, masses, and kinetic energies, the total charge in the inter-electrode gap should be equal to zero, and the PDs should have odd symmetry about the gap center.[3] Due to the symmetry, the number of solution branches turns out to be less than those for the general case $V \neq 0$, described in Ref. 6. Taking into account the symmetry, it also makes an opportunity to correct calculations when modeling time-dependent processes in the diode.

In Fig. 1, solution branches for $\Delta = 0$ and $\Delta = 0.01$ are shown. The solution branches for the mode without particle reflection from potential extrema are designated as n_k (index k is the number of extrema on the PD) in Fig. 1. In this case, $\eta_m > -(1-\Delta)^2/2$. In the case when electron reflection occurs, we call the potential minimum the virtual electron emitter (e-VE). Similarly, we call the potential maximum the virtual positron emitter (p-VE). There are two types of PD with particle reflection. When the e-VE is located to the left of the p-VE, the corresponding branches are designated d_k (the index k is the number of extrema on the PD lying between e-VE and p-VE) in Fig. 1. In the opposite case, when the p-VE is located to the left of the e-VE, the corresponding branches are designated $d_{i,j}$ (the index i is the
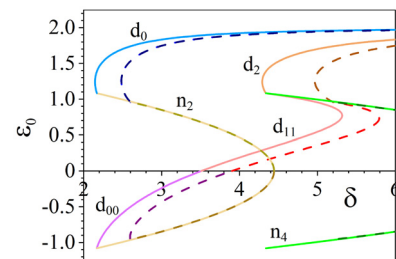

FIG. 1. Solution branches for $\Delta = 0$ (solid curves) and $\Delta = 0.01$ (dashed curves).

number of PD minima lying to the left of the p-VE, and index j is the number of PD maxima lying to the right of the e-VE) in Fig. 1. Due to the symmetry, in the case of $V = 0$, solutions belonging to branches n_k and d_k with $k = 0, 2, 4, \ldots$, as well as $d_{s,s}$ with $s = 0, 1, \ldots$ can only occur. Examples of PD corresponding to branches n_2 and d_0 are shown in Fig. 2(a), and for branches d_{00} and d_{11} in Fig. 2(b). The potential distributions for solutions without reflection were obtained in Ref. 7.

In the reflection mode, η_m varies in the interval $[-(1 + \Delta)^2/2, -(1 - \Delta)^2/2]$, and η_M varies in the interval

$[(1 - \Delta)^2/2, (1 + \Delta)^2/2]$ [see Figs. 2(a) and (b)]. The electron reflection starts at the point $\zeta_- < \zeta_m$, where the potential $\eta = -(1 - \Delta)^2/2$. In the region $(0, \zeta_-)$, there are electrons emitted from the left electrode and moving to the right boundary, as well as electrons reflected from the potential minimum. A flow of reflected electrons is formed in the region (ζ_-, ζ_m). In the region $(\zeta > \zeta_m)$, there are only electrons that have overcome the potential minimum η_m and are moving to the right electrode. Overcame and reflected positron flows are formed in a similar way. Particle densities are given by the following expressions:[8]

$$
n_e(\eta, \eta_m) = \frac{1}{2\Delta}
\begin{cases}
\sqrt{(1+\Delta)^2 + 2\eta} + \sqrt{-2\eta_m + 2\eta} \\
\quad - 2\sqrt{(1-\Delta)^2 + 2\eta}, & \zeta < \zeta_m, \eta > -\frac{1}{2}(1-\Delta)^2, \\
\sqrt{(1+\Delta)^2 + 2\eta} + \sqrt{-2\eta_m + 2\eta}, & \zeta < \zeta_m, \eta < -\frac{1}{2}(1-\Delta)^2, \\
\sqrt{(1+\Delta)^2 + 2\eta} - \sqrt{-2\eta_m + 2\eta}, & \zeta > \zeta_m,
\end{cases}
\tag{5}
$$

$$
n_p(\eta, \eta_M) = \frac{1}{2\Delta}
\begin{cases}
\sqrt{(1+\Delta)^2 - 2\eta} - \sqrt{2\eta_M - 2\eta}, & \zeta < \zeta_M, \\
\sqrt{(1+\Delta)^2 - 2\eta} + \sqrt{2\eta_M - 2\eta}, & \zeta > \zeta_M, \eta > \frac{1}{2}(1-\Delta)^2, \\
\sqrt{(1+\Delta)^2 - 2\eta} + \sqrt{2\eta_M - 2\eta} \\
\quad - 2\sqrt{(1-\Delta)^2 - 2\eta}, & \zeta > \zeta_M, \eta < \frac{1}{2}(1-\Delta)^2.
\end{cases}
\tag{6}
$$

Here ζ_m and ζ_M are the positions of the absolute potential minimum and maximum, respectively.

Let us find the PD for solutions corresponding to different branch types. The potential distributions corresponding to the n_s branches were calculated in Ref. 7. To calculate the PD corresponding to other branches, we multiply both sides of Eq. (4) by $\eta'/2$ and integrate once. This gives

$$
\eta' = \pm \left\{ (\eta_1')^2 + \frac{1}{3\Delta}[D(\eta) - D(\eta_1)] \right\}^{1/2},
$$
$$
D(\eta) = \int d\eta \left[n_e(\eta) - n_p(\eta) \right].
\tag{7}
$$

This relation is the basis on which it is possible to find and study the PD for all reflection branches.

A. d_0 branch

The characteristic PD for the d_0 branch is shown in Fig. 2(a) with a red curve. Since the solution is symmetrical to the middle of the inter-electrode gap, it is sufficient to consider the PD on the interval $(0, \delta/2)$.

To find the PD, we divide the interval $(0, \delta/2)$ into three segments: (1) from the left boundary ($\zeta = 0$) to the point ζ_-, where the reflection of electrons starts (potential $\eta = \eta_- = -(1 - \Delta)^2/2$); (2) from the point ζ_- to the position of the potential minimum ζ_m, where the reflection of electron finishes; and (3) from the point ζ_m to $\delta/2$, where all the unreflected electrons penetrate. In these three segments, the electron densities are described by various formulas [the first, second, and third of formula (5), respectively], which leads to different types of functions $D(\eta)$ in relation (7). The form of these functions is
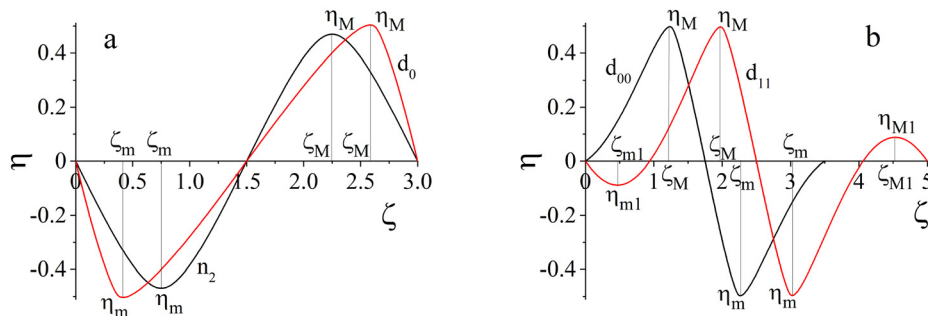

FIG. 2. Characteristic PD for n_2 (black) and d_0 (red curve) (a) and d_{00} (black) and d_{11} (red curve) (b) branches; $V = 0$.

TABLE I. Function $D(\eta)$ in different segments of interval $(0, \delta/2)$ for d_0 branch.

Segment	$D(\eta)$
$[0, \zeta_-]$	$D_1^e(\eta) = [(1+\Delta)^2 + 2\eta]^{3/2} + (-2\eta_m + 2\eta)^{3/2} - 2[(1-\Delta)^2 + 2\eta]^{3/2} + [(1+\Delta)^2 - 2\eta]^{3/2} - (-2\eta_m - 2\eta)^{3/2}$
$[\zeta_-, \zeta_m]$	$D_2^e(\eta) = [(1+\Delta)^2 + 2\eta]^{3/2} + (-2\eta_m + 2\eta)^{3/2} + [(1+\Delta)^2 - 2\eta]^{3/2} - (-2\eta_m - 2\eta)^{3/2}$
$[\zeta_m, \delta/2]$	$D_3^e(\eta) = [(1+\Delta)^2 + 2\eta]^{3/2} - (-2\eta_m + 2\eta)^{3/2} + [(1+\Delta)^2 - 2\eta]^{3/2} - (-2\eta_m - 2\eta)^{3/2}$

given in Table I. The positron density is determined by the first of formula (6).

The potential minimum value η_m is related to the field strength on the left boundary ε_0. To find this connection, we need to use relation (7) with the function D_1^e in the interval $[0, \zeta_-]$ and D_2^e in the interval $[\zeta_-, \zeta_m]$. This gives the relation

$$\varepsilon_0 = \left(\frac{1}{3\Delta}\right)^{1/2}\left\{D_1^e(0) - D_1^e\left[-(1-\Delta)^2/2\right] \right. $$
$$\left. + D_2^e\left[-(1-\Delta)^2/2\right] - D_2^e(\eta_m)\right\}^{1/2}. \tag{8}$$

Note that the mode with particle reflection goes to that without reflection (and the d_0 branch goes into the n_2 one) in the case when $\eta_m = \eta_- = -(1-\Delta)^2/2$ and $\zeta_m = \zeta_-$. Wherein in formula (8) the last two terms in the expression under square root cancel each other out, and the field strength at the left boundary turns out to be equal to

$$\varepsilon_{0,min} = \left(\frac{1}{3\Delta}\right)^{1/2}\left\{D_1^e(0) - D_1^e\left[-(1-\Delta)^2/2\right]\right\}^{1/2}$$
$$= \left(4 - \frac{4}{3}\left\{\sqrt{2}\left[1 + \frac{1+\Delta^2}{1-\Delta+\sqrt{1+\Delta^2}}\right]\right.\right.$$
$$\left.\left. + 2\sqrt{\Delta} - \sqrt{2}\,\Delta - \Delta^2\right\}\right)^{1/2}. \tag{9}$$

The PD on each of the segments is obtained by integrating relation (7) with the corresponding function D from the boundary of the segment up to a variable upper limit ζ, where the potential is equal to $\eta(\zeta)$. The resulting dependencies $\zeta(\eta)$ are given in Table II. Note that in segments 2 and 3, one of the boundaries is the point of the potential minimum, at which the derivative vanishes and its value is not included in the integrand function.

TABLE II. Dependence $\zeta(\eta)$ in different segments of interval $(0, \delta/2)$ for d_0 branch.

Segment	$\zeta(\eta)$
$[0, \zeta_-]$	$\zeta = -\int_0^\eta \left\{\varepsilon_0^2 + [D_1^e(x) - D_1^e(0)]/(3\Delta)\right\}^{-1/2}dx = \zeta_1^e(\eta)$
$[\zeta_-, \zeta_m]$	$\zeta = \zeta_m - \sqrt{3\Delta}\int_{\eta_m}^\eta [D_2^e(x) - D_2^e(\eta_m)]^{-1/2}dx = \zeta_m - \zeta_2^e(\eta)$
$[\zeta_m, \delta/2]$	$\zeta = \zeta_m + \sqrt{3\Delta}\int_{\eta_m}^\eta [D_3^e(x) - D_3^e(\eta_m)]^{-1/2}dx = \zeta_m + \zeta_3^e(\eta)$

The lengths of the segments into which the interval $[0, \delta/2]$ is divided are equal to $\zeta_1^e(\eta_-)$, $\zeta_2^e(\eta_-)$, and $\zeta_3^e(0)$, respectively. Inter-electrode distance is given as

$$\delta = 2\left\{\int_{-(1-\Delta)^2/2}^0 \frac{dx}{\left\{\varepsilon_0^2 + [D_1^e(x) - D_1^e(0)]/(3\Delta)\right\}^{1/2}}\right.$$
$$+ \sqrt{3\Delta}\left[\int_{\eta_m}^{-(1-\Delta)^2/2} \frac{dx}{[D_2^e(x) - D_2^e(\eta_m)]^{1/2}}\right.$$
$$\left.\left. + \int_{\eta_m}^0 \frac{dx}{\left\{[D_3^e(x) - D_3^e(\eta_m)]^{1/2}\right\}}\right]\right\}. \tag{10}$$

Note that $\zeta_2^e(\eta_m)$ is the length of the interval within which particles are reflected. Taking into account the connection (8) between η_m and ε_0, expression (10) is the equation of the d_0 branch on the (ε_0, δ) plane.

An example of solution branches for $\Delta = 0.01$ is shown in Fig. 1 in dashed lines. It can be seen that the n_2 branch smoothly transforms into the d_0 one as ε_0 increases. The latter, with an increase in ε_0, first goes in the direction of decreasing δ, but then turns and goes in the direction of increasing δ. Thus, there is a left bifurcation point δ_{BF}, which determines the left boundary of branch d_0 along δ. To find the dependence of the point δ_{BF} on the spread value Δ, we have calculated this branch for a number of Δ values. The results are shown in Fig. 3. It can be seen that the bifurcation point shifts toward increasing δ with rising in spread value.

In Table III, δ_{BF} point coordinates for three spread values are tabulated. It turns out that this shift quite well satisfies the law: $\delta_{BF}^{(a)}(\Delta) = \delta_{BF}(0) + (10/3)\sqrt{\Delta}$ (cf. third and sixth columns of Table III).
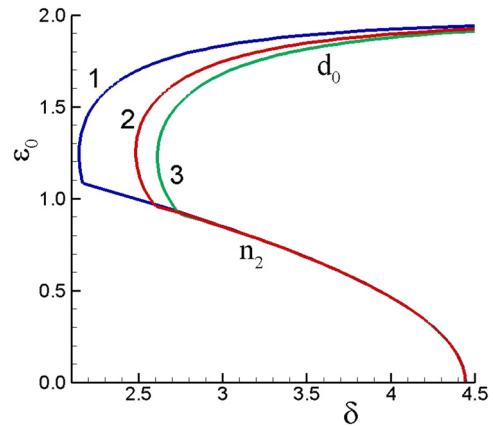

FIG. 3. The n_2 and d_0 branches built for three spread values of VDF: $\Delta = 0$, 0.01, and 0.02.

TABLE III. Bifurcation point δ_{BF} coordinate dependence on Δ.

n	Δ	δ_{BF}	$\varepsilon_{0,BF}$	$\eta_{min,BF}$	$\delta_{BF}^{(a)}$
1	0.00	2.1444	1.2412	-0.5000	2.1444
2	0.01	2.4835	1.2579	-0.49425	2.4777
3	0.02	2.6116	1.2283	-0.4886	2.6158

B. d_{00} branch

The d_{00} branch corresponds to PD in which, unlike the d_0 branch, the p-VE is located to the left of the e-VE [cf. Fig. 2(b), black curve, and Fig. 2(a), red curve]. This branch lies entirely within the negative ε_0 region. It starts at the point where n_2 branch ends. Here, the potential value at the maximum $\eta_M = \eta_+ = (1-\Delta)^2/2$ is the smallest for the entire branch and corresponds to the boundary of the mode with reflection. Further, as ε_0 increases, η_M value grows, while remaining less than $(1+\Delta)^2/2$, up to the point where ε_0 vanishes, and the d_{00} branch goes into d_{11} branch.

Considering the d_0 branch is also sufficient to find the PD within the interval $(0, \delta/2)$. Let us divide this interval into three segments: (1) $[0, \zeta_M]$, here the potential varies within $[0, \eta_M]$, in this segment only positrons that have overcome the potential barrier occur; (2) $[\zeta_M, \zeta_+]$, here the potential varies within area $[\eta_M, (1-\Delta)^2/2]$, a flow of reflected positrons is formed in this segment; and (3) $[\zeta_+, \delta/2]$, here the potential varies within area $[(1-\Delta)^2/2, 0]$, in this segment there are two positron flows: emitted from the right electrode and reflected. The positron density within these three regions is determined by the first, second, and third of formula (6), respectively. All three segments contain both direct and reflected electrons, whose densities are determined by the first of formula (5). Forms of the function $D(\eta)$ for the segments are given in Table IV.

The relation between ε_0 and η_M is found using a relation (7) within the $[0, \zeta_M]$ interval and is given as follows:

$$\varepsilon_0 = -\left\{ \left[D_1^p(0) - D_1^p(\eta_M)\right]/(3\,\Delta) \right\}^{1/2}. \tag{11}$$

When $\eta_M = (1-\Delta)^2/2$, the ε_0 value is the smallest one. It coincides in absolute value with $\varepsilon_{0,min}$ determined by formula (9) and is of the opposite sign.

At $\varepsilon_0 = 0$, the η_M value reaches its greatest value, which is determined by

$$\left[(1+\Delta)^2 + 2\,\eta_M\right]^{3/2} + (4\,\eta_M)^{3/2} - 2\left[(1-\Delta)^2 + 2\,\eta_M\right]^{3/2}$$
$$+ \left[(1+\Delta)^2 - 2\,\eta_M\right]^{3/2} - 12\,\Delta - 4\,\Delta^3 = 0. \tag{12}$$

The PD in different segments is obtained by integrating relation (7) in the same way as for the d_0 branch and is shown in Table V.

The segment lengths are $\zeta_1^p(\eta_m)$, $\zeta_2^p(\eta_+)$, and $\zeta_3^p(0)$. The interelectrode gap value is equal to

$$\delta = 2\left\{ \int_0^{\eta_M} \frac{dx}{\left\{\varepsilon_0^2 + \left[D_1^p(x, \eta_M) - D_1^p(0, \eta_M)\right]/(3\,\Delta)\right\}^{1/2}} \right.$$
$$+ \int_{(1-\Delta)^2/2}^{\eta_M} \frac{\sqrt{3\,\Delta}\,dx}{\left[D_2^p(x) - D_2^p(\eta_M)\right]^{1/2}} + \int_0^{(1-\Delta)^2/2}$$
$$\left. \times \frac{\sqrt{3\,\Delta}\,dx}{\{D_3^p(x) - D_3^p\left[(1-\Delta)^2/2\right] + D_2^p\left[(1-\Delta)^2/2\right] - D_2^p(\eta_M)\}^{1/2}} \right\}. \tag{13}$$

The d_{00} branch is built by varying the parameter ε_0 from the smallest value equal to $-\varepsilon_{0,min}$ (9) to 0, or by varying η_M from $(1-\Delta)^2/2$ to the largest value determined from (12).

C. d_{11} branch

The d_{11} branch continuously extends d_{00} one into the region of positive ε_0 values. It includes PDs whose minimum η_{m1} is located near

TABLE IV. Function $D(\eta)$ in different segments of interval $(0, \delta/2)$ for d_{00} branch.

Segment	$D(\eta)$
$[0, \zeta_M]$	$D_1^p(\eta) = \left[(1+\Delta)^2 + 2\,\eta\right]^{3/2} + (2\,\eta_M + 2\,\eta)^{3/2} - 2\left[(1-\Delta)^2 + 2\,\eta\right]^{3/2} + \left[(1+\Delta)^2 - 2\,\eta\right]^{3/2} - (2\,\eta_M - 2\,\eta)^{3/2}$
$[\zeta_M, \zeta_+]$	$D_2^p(\eta) = \left[(1+\Delta)^2 + 2\,\eta\right]^{3/2} + \left[2\,(\eta_M + \eta)\right]^{3/2} - 2\left[(1-\Delta)^2 + 2\,\eta\right]^{3/2} + \left[(1+\Delta)^2 - 2\,\eta\right]^{3/2} + (2\,\eta_M - 2\,\eta)^{3/2}$
$[\zeta_+, \delta/2]$	$D_3^p(\eta) = \left[(1+\Delta)^2 + 2\,\eta\right]^{3/2} + \left[2\,(\eta_M + \eta)\right]^{3/2} - 2\left[(1-\Delta)^2 + 2\,\eta\right]^{3/2} + \left[(1+\Delta)^2 - 2\,\eta\right]^{3/2} + \left[2\,(\eta_M - \eta)\right]^{3/2} - 2\left[(1-\Delta)^2 - 2\,\eta\right]^{3/2}$

TABLE V. Dependence $\zeta(\eta)$ in different segments of $(0, \delta/2)$ interval for d_{00} branch.

Segment	$\zeta(\eta)$
$[0, \zeta_M]$	$\zeta = \int_0^{\eta} \left\{\varepsilon_0^2 + \left[D_1^p(x) - D_1^p(0)\right]/(3\,\Delta)\right\}^{-1/2} dx = \zeta_1^p(\eta)$
$[\zeta_M, \zeta_+]$	$\zeta = \zeta_M + \sqrt{3\,\Delta} \int_\eta^{\eta_M} \left[D_2^p(x) - D_2^p(\eta_M)\right]^{-1/2} dx = \zeta_M + \zeta_2^p(\eta)$
$[\zeta_+, \delta/2]$	$\zeta = \zeta_+ + \sqrt{3\,\Delta} \int_\eta^{(1-\Delta)^2/2} \left\{D_3^p(x) - D_3^p[(1-\Delta)^2/2] + D_2^p[(1-\Delta)^2/2] - D_2^p(\eta_M) \right\}^{-1/2} dx = \zeta_+ + \zeta_3^p(\eta)$

16 October 2024 11:49:50

the left boundary. Its absolute value is less than the absolute minimum $|\eta_m|$ [Fig. 2(b), red curve]. To the right of the minimum, the potential grows with increasing coordinate and reaches a maximum η_M. The p-VE is located here. Then the potential decreases, reaches absolute minimum η_m, and so on. As well as on the d_{00} branch, electron reflection occurs to the right of the middle of the gap, i.e., at $\zeta > \delta/2$.

Within the segment $(0, \zeta_M)$, Eq. (12) with the function $D(\eta) \equiv D_1^p(\eta)$ is still valid. Moreover, in the region lying between the point behind the local minimum ζ_0, where the potential vanishes, and $\delta/2$, the equations and formulas for the PD given above for the d_{00} branch remain valid. The ε_0 value included in them now makes sense of the field strength at point ζ_0. However, the PD in the segment $(0, \zeta_0)$ is symmetrical with respect to the local minimum point ζ_{m1}; therefore, the field strength at the point ζ_0 is equal to $-\varepsilon_0$, and the value of ε_0^2 in formulas describing the PD within the interval $(\zeta_0, \delta/2)$ does not change. Therefore, it is only sufficient to find PD within the region $(0, \zeta_0)$.

The relation between η_{m1} and η_M is obtained from the condition that the total charge in the layer (ζ_{m1}, ζ_M) is equal to zero:

$$D_1^p(\eta_M) - D_1^p(\eta_{m1}) = 0. \tag{14}$$

The minimum value $|\eta_{m1}| = 0$ corresponds to the maximum η_M value, which is determined from

$$D_1^p(\eta_M) - D_1^p(0) = 0. \tag{15}$$

The maximum value of $|\eta_{m1}|$ is obtained from the minimum value of $\eta_M = (1 - \Delta)^2/2$ and is determined by

$$D_1^p[(1 - \Delta)^2/2] - D_1^p(\eta_{m1}) = 0. \tag{16}$$

The relation between η_{m1} and ε_0 is given by

$$\varepsilon_0 = \left\{ \frac{1}{3\Delta} \left[D_1^p(0) - D_1^p(\eta_{m1}) \right] \right\}^{1/2}. \tag{17}$$

The potential distribution in the region $(0, \zeta_{m1})$ is given by

$$\zeta = \int_0^\eta \frac{dx}{\{\varepsilon_0^2 + [D_1^p(x) - D_1^p(0)]/(3\Delta)\}^{1/2}}. \tag{18}$$

The coordinate of the local minimum ζ_{m1} is obtained from (18) with $\eta = \eta_{m1}$. Within the segment (ζ_{m1}, ζ_0), the PD is found using the above-mentioned property of symmetry about the straight line $\zeta = \zeta_{m1}$.

Thus, the equation for d_{11} branch is as follows:

$$\begin{aligned} \delta = 2 \Bigg\{ &2 \int_0^{\eta_{m1}} \frac{dx}{\{\varepsilon_0^2 + [D_1^p(x) - D_1^p(0)]/(3\Delta)\}^{1/2}} \\ &+ \int_0^{\eta_M} \frac{dx}{\{\varepsilon_0^2 + [D_1^p(x) - D_1^p(0)]/(3\Delta)\}^{1/2}} \\ &+ \int_{(1-\Delta)^2/2}^{\eta_M} \frac{\sqrt{3\Delta}\, dx}{[D_2^p(x) - D_2^p(\eta_M)]^{1/2}} + \int_0^{(1-\Delta)^2/2} \\ &\times \frac{\sqrt{3\Delta}\, dx}{\{D_3^p(x) - D_3^p[(1-\Delta)^2/2] + D_2^p[(1-\Delta)^2/2] - D_2^p(\eta_M)\}^{1/2}} \Bigg\}. \end{aligned} \tag{19}$$

Here η_M value relates to ε_0 via Eqs. (14) and (17).

Varying $|\eta_{m1}|$ from 0 (with $\varepsilon_0 = 0$) to the maximum value determined by formula (16), we construct d_{11} branch. Figure 1 shows the solution branches for diodes with spreads $\Delta = 0$ and $\Delta = 0.01$ in the region of $\delta < 6$. Comparison of solid and dashed curves shows that a slight spread of the VDF leads to a shift of these dependencies to the right and a slight stretch along the δ axis.

III. NUMERICAL CALCULATIONS OF INSTABILITY DEVELOPMENT

When researching stationary solution stability features in electron–positron diode, we study the evolution of a small perturbation of the stationary electric field distribution. If the solution turns out to be unstable, the perturbation evolves to a solution different from the steady state one. In the opposite case, the process returns to the initial state. For simulation, we used two different numerical codes: PIC-code (implementing calculations by the particle method) and EK-code.

The PIC-code simulates the movement of a huge number of electrons emitted from the left boundary and positrons emitted from the right boundary, and moving under electric field set at the grid nodes. The grid consists of N_ζ nodes with an equal distance h_ζ between them. The charge density at the nodes is calculated in accordance with the "cloud-in-cell" model (linear particle contribution to the density at neighboring nodes),[9] unit density corresponds to N_0 particles in a cell. The electric field at the nodes is found as a solution of the Poisson equation, and between the nodes the field is approximated by a linear function.[9] The position of a particle at each subsequent time moment is calculated by the "leapfrog" method,[9] and the time step h_τ is chosen to be constant. At each step, particles that reach any electrode are removed from the calculation, and particles that fly out from the electrodes with random velocities distributed in accordance with a given VDF are added. In the calculations described below, a uniform velocity distribution at the electrodes was specified in the interval $[1 - \Delta, 1 + \Delta]$ for electrons and in the interval $[-(1 + \Delta), -(1 - \Delta)]$ for positrons. The moment of particle departure from the electrode was considered random and uniformly distributed within the time step.

The numerical algorithm implemented in the EK-code is described in detail in the papers,[8,10] where it is modified to calculate processes in a diode with counter flows of negatively and positively charged particles. At each time step, the charged particle VDF, their densities, and electric field distribution are sequentially determined. The particle VDF at a given point (τ^i, ζ_k) is built by calculating a set of trajectories ending at this point. The computation is carried out backward in time from τ^i up to the moment τ_0 when the particle left the electrode. In this case, the electric field distributions at all previous times $(\tau < \tau^i)$ are considered known. The field distribution at each time moment is found from the Poisson equation, into the right side of which the electron and positron densities calculated for this time moment are substituted. Since the distribution of the electric field is unknown at the last time interval (τ^{i-1}, τ^i), its extrapolation to this interval is used when the densities are calculated. Then iterations are carried out with alternate recalculation of the field and particle densities.

When a small perturbation evolution was calculated by the EK-code, the electric field distributions were set equal to the stationary distribution over a sufficiently long period of time τ_s, so that particle density distribution equal to the stationary one had time to adjust in the inter-electrode gap. Then, at the time step immediately following
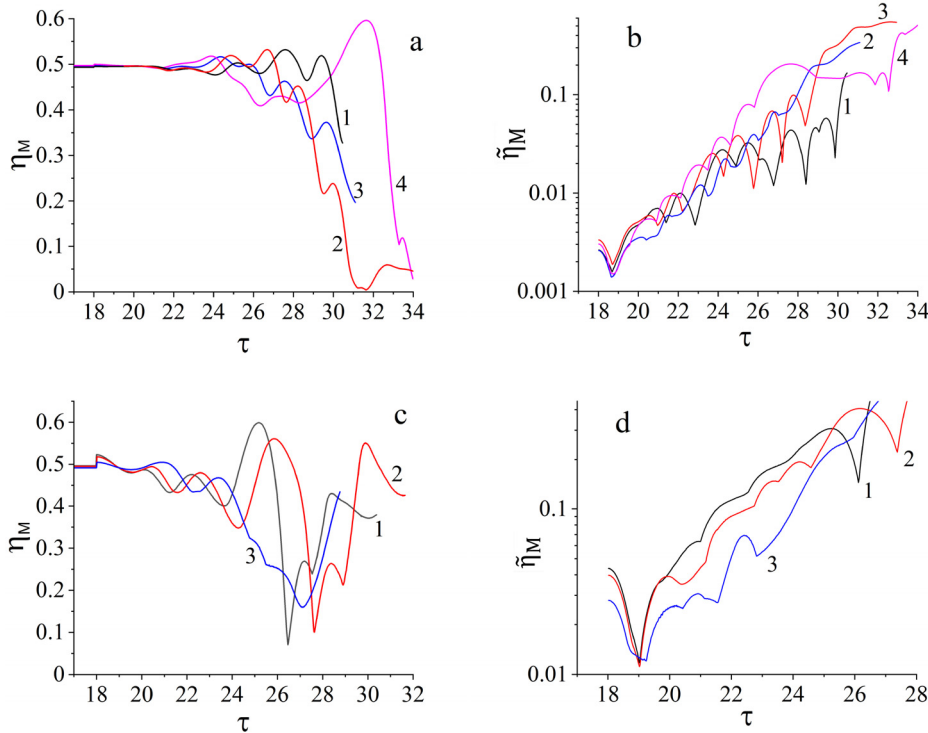
FIG. 4. Time dependencies of the potential maximum $\eta_M(\tau)$ (a) and (c) and the potential perturbation $\tilde{\eta}_M(\tau)$ (b) and (d) for solutions corresponding to d_{00} (a) and (b) and d_{11} (c) and (d) branches: $\delta = 2.7$ (1), 2.8 (2), 3.0 (3), and 3.5 (4) for d_{00} branch, $\delta = 5$ (1) and 5.6 [(2)—a point on the lower part of the branch, (3)—on the upper part of the branch] for d_{11} branch; $\Delta = 0.01$.

the moment $\tau = \tau_s$, the time-dependent self-consistent computation of the field and particle distributions starts. In this case, at the moment $\tau > \tau_s$, a small random perturbation of the field distribution arose due to the finite accuracy of the calculations. However, sometimes another initial condition is used: during the time interval $(0, \tau_s)$, an exponentially growing sinusoidal perturbation with an amplitude much less than unity was superimposed on the stationary field distribution.

When using the PIC-code, in some cases, the field distribution within the diode was also set equal to the stationary distribution during the time interval $(0, \tau_s)$, and after that the time-dependent self-consistent calculation started. In other cases, the self-consistent calculation started at the time $\tau = 0$, while at each point in the gap, a stationary field distribution (with or without a perturbation imposed on it) and the initial particle VDFs corresponding to the initial field distribution were specified. At each point, the initial VDF was of rectangular distribution form: the particles were uniformly distributed over velocities within the interval, the boundaries of which were determined from the stationary law of energy conservation.

First, we investigated the stability features of solutions belonging to d_{00} and d_{11} branches. In these calculations, the velocity spread was $\Delta = 0.01$. The d_{11} branch continues the d_{00} branch as the interelectrode gap length δ increases. Diodes with δ values equal to 2.7, 2.8, 3.0, and 3.5 were considered for the d_{00} branch, and $\delta = 5.0$ and 5.6 were considered for the d_{11} branch. These values cover almost the entire range of possible diode lengths for which solutions of these types exist. Note that at $\delta = 5.6$ there are two stationary solutions belonging to the branch d_{11}, which differ in the value of ε_0 (see Fig. 1). In all the cases studied, the solutions turned out to be unstable.

Figure 4 shows the dependencies of the potential maximum value η_M and the potential perturbation amplitude $\tilde{\eta}_M$ on time at the initial stage of the process, obtained as a result of the EK-code modeling. The dependencies in Figs. 4(a) and 4(b) relate to the d_{00} branch. In all cases, $\eta_M(\tau)$ oscillates, and the oscillation amplitude grows with time. During the oscillation process, the PD shape is rearranged several times, wherein the absolute maximum of the distribution is located either to the left or to the right of the diode middle. The growth of the perturbation amplitude $\tilde{\eta}_M$ for values of the order of 0.01–0.1 is close to exponential: for $\delta = 3.5$, the envelope $\tilde{\eta}_M$ is a straight line on a logarithmic scale, and for smaller values, length dependence is less regular [Fig. 4(b)]. Figures 4(c) and 4(d) show the dependencies of $\eta_M(\tau)$ and $\tilde{\eta}_M(\tau)$ for solutions corresponding to d_{11} branch. It can be seen that at the initial stage oscillations $\eta_M(\tau)$ occur, and the envelope of the dependence $\tilde{\eta}_M(\tau)$ resembles an exponential.

These conclusions were confirmed by PIC-code calculations performed for the same diode lengths with varying shapes of potential perturbation at the initial time (sinusoidal or random due to errors in the numerical calculation). In all cases, the PD turned out to be unstable, and increasing oscillation amplitudes were observed at the initial stage of evolution; however, shape and amplitude of the oscillations strongly depended on the initial perturbation. Nevertheless, in all cases, the oscillation amplitude increased more or less exponentially with similar exponents. Figure 5 shows the PIC-code results for the initial stage of the PD evolution for the solutions belonging to the d_{00} branch for $\delta = 3.5$ and d_{11} one for $\delta = 5.0$.

The time dependence of the field strength at the left electrode $\varepsilon(\tau, 0)$ does not coincide with the dependencies $\eta_M(\tau)$, $\tilde{\eta}_M(\tau)$, which is natural, since at this stage the distribution form is continuously restructuring. Note that different scenarios for the development of the initial perturbation are possible, so we can only state the instability of the solutions studied, but their change over time
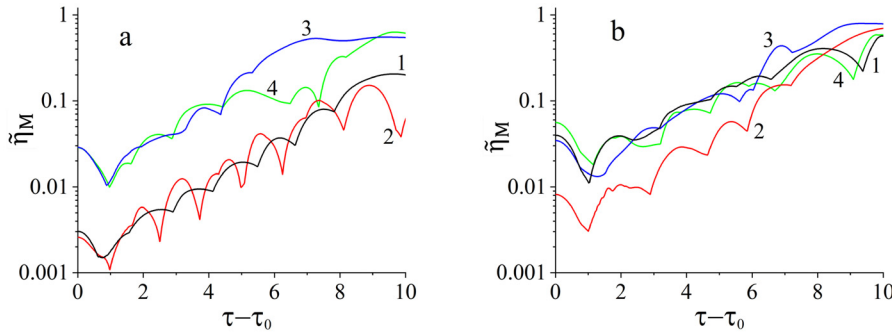
FIG. 5. Time dependencies of potential maximum perturbation $\tilde{\eta}_M(\tau)$ for solutions corresponding to d_{00} branch at $\delta = 3.5$ (a) and d_{11} one at $\delta = 5$ (b), calculated by the EK-code (1) and the PIC-code with different shapes of the initial perturbation: random, caused by numerical errors, (2) and sinusoidal with a maximum shift of 0.001 up (3) and down (4); $\Delta = 0.01$.

under various forms of perturbation may differ from the dependencies in Fig. 4.

We studied the stability features of solutions belonging to the d_0 branch in its upper part (above the bifurcation point) for several values of velocity spread: $\Delta = 0.005, 0.01, 0.015, 0.02$. As in the calculations for the d_{00} and d_{11} branches, the time dependence of the maximum deviation of the solution from the stationary one $\tilde{\eta}_M$ was analyzed. In all cases, it was found that when the diode length was less than a certain threshold length δ_{th}^d, the perturbation amplitude decreased with time, i.e., stationary solutions were stable. When δ exceeds the threshold value δ_{th}^d, the perturbation increases with time, i.e., the solutions become unstable. In this case, for almost all studied diode lengths (with the exception of a small part at the very beginning of the d_0 branch), at the initial stage of the perturbation evolution after a short transient process, it is possible to identify a time interval where the envelope of the $\eta_M(\tau)$ dependence is well approximated by the exponential, i.e., this dependence has the character of exponentially dumping or increasing oscillations of a regular sinusoidal shape with a constant frequency:

$$\eta_M(\tau) = \eta_{M0} + C \exp(\Gamma\tau) \sin(\omega\tau + \phi). \quad (20)$$

Note that the time dependencies of $\varepsilon(\tau, 0)$ at the linear stage of the disturbance development have the same character. It is shown in Fig. 6 for $\delta = 2.8$ and 3.0 for $\Delta = 0.01$.

In addition, the stability features of the solution belonging to the lower part of the d_0 branch (below the bifurcation point) were studied at $\delta = 2.55$, $\varepsilon_0 \approx 1.027$ for $\Delta = 0.01$. The solution turned out to be unstable; the process of the perturbation evolution ended with a uniform distribution of the potential.

Based on the calculation results, we determined the growth rates Γ and the oscillation frequencies ω in Eq. (20). The $\Gamma(\delta)$ dependencies obtained using the EK-code are presented in Fig. 7(a). The oscillation frequency changes slightly in the studied range of diode lengths, since it is determined by the characteristic time of flight of charged particles through the diode.

The stability threshold δ_{th}^d (the value of δ at which the growth rate Γ changes sign) shifts to the right as Δ increases. The dependence of δ_{th}^d on Δ for small Δ can be approximated by a linear function: $\delta_{th}^d = 2.6 + 30\,\Delta$ [Fig. 7(b)]. Note that we determine the position of the stability threshold with an accuracy of 0.05.

The calculations have shown that in diodes with a length δ exceeding the stability threshold, the exponential growth of the oscillation amplitude continues to values of the order of several hundredths. After this, the increase in amplitude begins to slow down, and

eventually the oscillations turn into periodic ones. At values of δ being near the stability threshold, the dependencies $\eta(\tau)$ and $\zeta(\tau)$ are close to sinusoidal; with increasing δ, the shape of the oscillations is distorted.

We built the dependencies $\eta_M(\zeta_M)$ (the maximum value on the PD η_M and its position ζ_M depend on time as a parameter). When the solution is unstable, this dependence is an unwinding spiral (with turns of irregular shape) at the stage of exponential growth of the oscillation amplitude. Then the distance between the turns gradually decreases, and, in the end, the curve reaches a closed loop that corresponds to steady-state nonlinear oscillations. Such loops are shown in Figs. 8(a) and 8(b) for $\delta = 3$ and 3.5.

Note that a number of other time-dependent processes, which we also simulated, also end in nonlinear oscillations. In particular, at $\delta = 3.0$ and 4.0, we considered an evolution of the perturbation of steady states corresponding to the n_2 branch for various types of perturbation. In one of the possible scenarios for the development of the perturbation the process ended with nonlinear periodic oscillations in the vicinity of the d_0 branch.[7] The same oscillations were established in calculations with a zero initial condition, when it was assumed that before the start of the calculation, there were no charged particles in the diode. The cycle of steady-state oscillations of the PD maximum at $\delta = 4.0$ in the case of the absence of particles in the diode at the initial time is shown in Fig. 8(c).

We plotted the dependence of the amplitude of steady-state oscillations on the diode length for two VDF half-width values: $\Delta = 0.01$ and 0.015. In the vicinity of the threshold, the amplitude of oscillations grows with increasing δ. Figure 9 shows how the value of the oscillation amplitude $\eta_M^{max}(\delta) - \eta_M^{min}$ increases as δ moves away from the stability threshold $\delta - \delta_{th}^d$. On a logarithmic scale, it is clear that this is a power-law dependence with an exponent close to 0.5. This indicates that the position of the stability threshold δ_{th}^d is the Hopf bifurcation point.

In the paper,[11] where nonlinear oscillations in a diode with flows of electrons and ions were studied, it has been proven that long-lived ions appear in the plasma. These ions "live" for several periods of plasma oscillation, being, in a way, captured by an oscillating ionic potential barrier that periodically appears on their way. It is natural to assume that similar processes should occur in a diode with electron–positron plasma, and long-lived particles of both signs can also exist. To verify this assumption, we plotted the electron and positron distribution functions in terms of velocities and coordinates at different times and made sure that, as in the case of electron–ion plasma, the VDF at each point of the diode is a set of narrowing velocity intervals
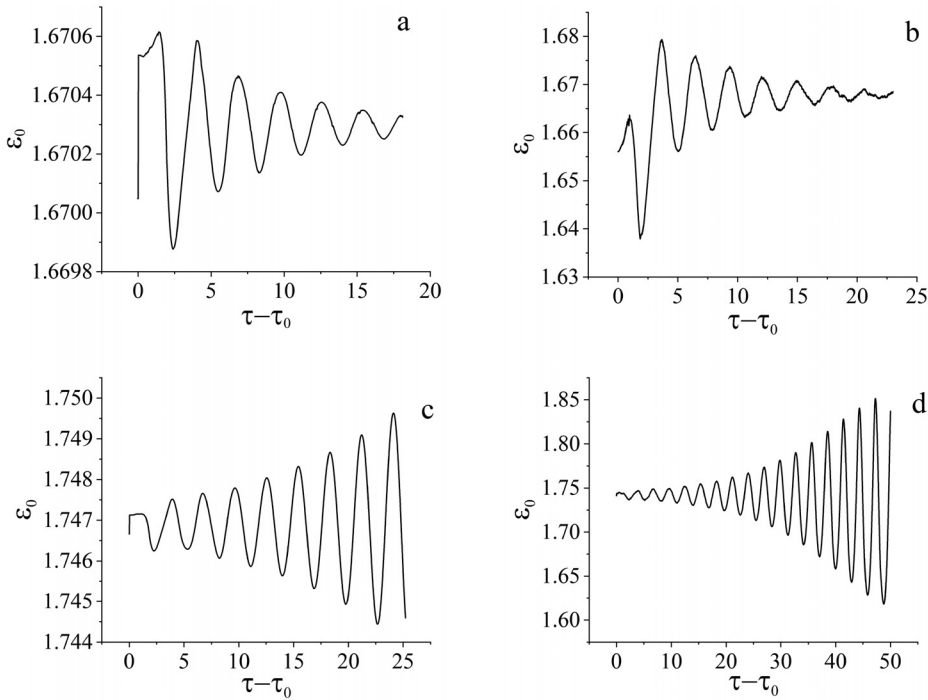
FIG. 6. Time dependencies of the field strength at the left electrode $\varepsilon_0(\tau)$ for diode lengths $\delta = 2.8$ (a) and (b) and 3.0 (c) and (d), obtained using the EK-code (a) and (c) and PIC-code (b) and (d) at the initial stage of the disturbance development for solutions corresponding to the d_0 branch; $\Delta = 0.01$.

with a constant value of the VDF, outside of which this function is equal to zero. Over time, the number of intervals is getting larger and larger, which means the capture of charged particles into dynamic potential wells formed by moving PD extrema. Figure 10 shows the positron VDF at time moments corresponding to different points of the cycle shown in Fig. 8(b). On the scale used, one can distinguish only the widest intervals; examples of intervals structure at a fixed coordinate are shown in the insets. On panel (a), the interval *1a* splits to *4a, 5a* at $\zeta = 0.86$, and the interval *6a* splits to *7a, 8a* at $\zeta = 2.87$. On panel (b), the interval *1b* splits to *8b,9b* at $\zeta = 2.47$. Remember that the same numbers on panels (a) and (b) designate different intervals, we did not try to set up a correspondence between the panels.

The presence of several narrow velocity intervals is illustrated in Tables VI and VII. The tables show the boundaries of the positron velocity intervals in the cross sections $\zeta = 0.42$ and $\zeta = 3.22$ at the

bottom point of the cycle shown in Fig. 8(b). The interval numbers in the tables correspond to curve numbers in Fig. 10(b). At $\zeta = 3.22$, the interval *5b* is too narrow to determine its boundaries correctly ($\sim 10^{-8}$), so we do not present their values in Table VII. The interval widths and the distance between intervals decrease exponentially with the velocity increase, except for the lowest intervals, where particles cannot yet be considered as long-lived. The same dependence had been observed in the case of long-lived ions.[11]

Figure 10 and Tables VI and VII show how the phase plane transforms over the period of oscillation. The electron VDF can be obtained by mirroring the positron VDF relative to the diode middle.

IV. CONCLUSION

We investigated the stability features of main steady state types in a diode with electrons and positrons counter flows.[3,6,7] In the latter
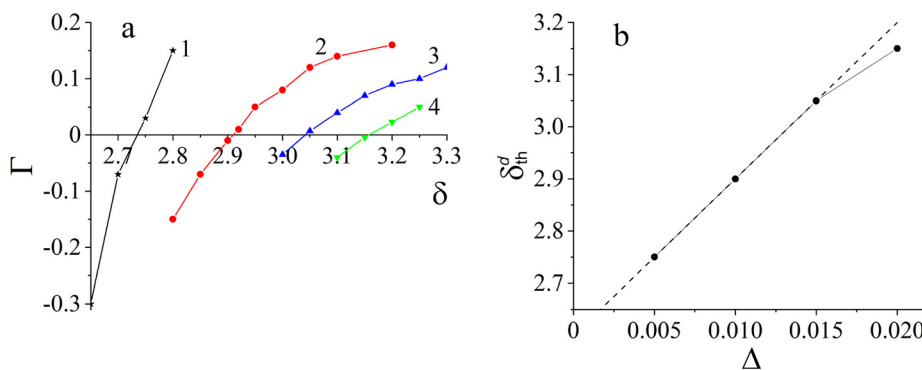

FIG. 7. (a) Values of the growth rate Γ when approximating $\eta_M(\tau)$ by Eq. (20) at the initial stage of the perturbation development for solutions belonging to the d_0 branch, for a number of VDF half-width values: $\Delta = 0.005$ (1), 0.01 (2), 0.015 (3), and 0.02 (4). (b) Dependence of the stability threshold of stationary solutions belonging to the d_0 branch on the VDF width Δ.
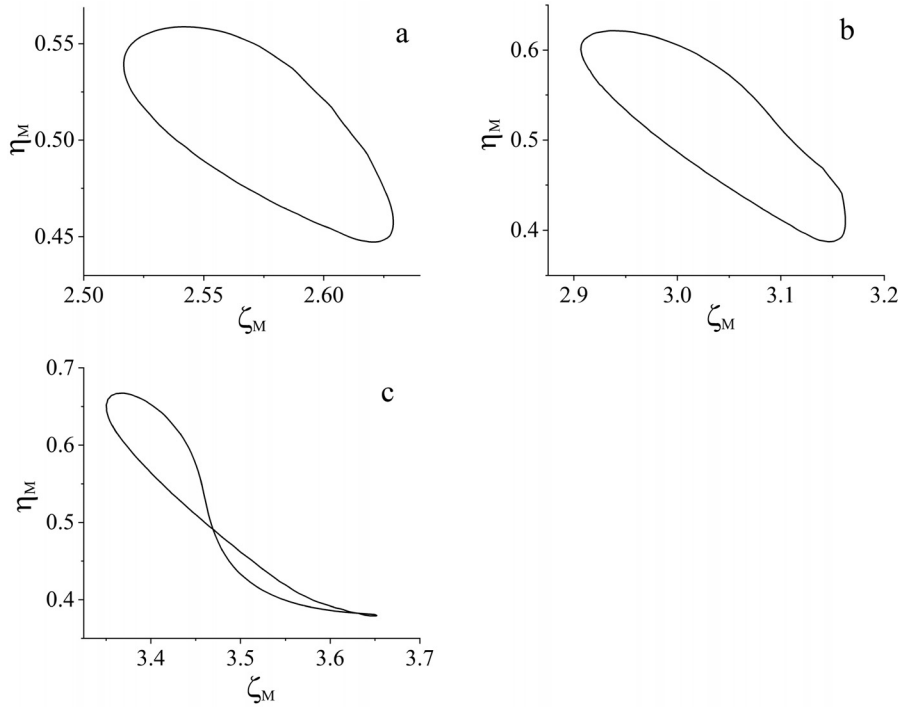
FIG. 8. Dependence of the maximum potential $\eta_M(\tau)$ on its position $\zeta_M(\tau)$ for one cycle of steady oscillations for diode lengths $\delta = 3$ (a), 3.5 (b), and 4.0 (c) and $\Delta = 0.01$.

two papers, this problem was studied for the regime without reflection of charged particles from potential extrema, i.e., for n_k branches with $k = 0, 2, 4, \ldots$. It was established analytically and confirmed numerically that for homogeneous solutions there is a threshold for the dimensionless inter-electrode gap δ (or, what is the same, for the current density), above which instability develops in the diode. The threshold δ_{th}^0 turned out to be equal to $\sqrt{2}\,\pi\,\lambda_D$, which is $\sqrt{2}$ higher than the known Pierce one.[12] On the other hand, all inhomogeneous stationary solutions turn out to be unstable with respect to small perturbations. In this case, the time-dependent process either ends in a new state, characterized by nonlinear oscillations that occur around the stationary solution corresponding to the d_s branches, or reaches a homogeneous solution (if $d < \sqrt{2}\,\pi\,\lambda_D$).
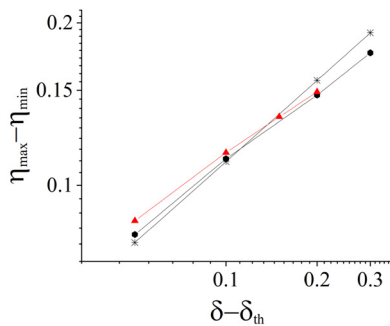

FIG. 9. Dependence of the steady-state oscillation amplitude on the difference $\delta - \delta_{th}^d$ for two values of Δ: $\Delta = 0.01$ (circles) and $\Delta = 0.015$ (triangles). The asterisks correspond to the approximation dependence $(\delta - \delta_{th}^d)^{1/2}$.

In the paper, we studied the stability features of steady states in the regime with particle reflection from potential barriers, i.e., solutions corresponding to d_0, d_{00}, and d_{11} branches. Since the studies were carried out numerically, not a δ-shaped VDF, but a distribution function with a small spread Δ in velocities was used. All stationary solutions have been described. They qualitatively coincided with that corresponding to the δ-shaped VDF. Distinction is observed only in the vicinity of the left bifurcation point (see Fig. 3). A law has been found according to which the bifurcation point shifts along δ as the spread Δ increases.

The calculations of stationary solution small perturbation development were performed. It has been established that the solutions for the d_{00} and d_{11} branches are unstable, while solutions from the d_0 branch turn out to be stable when the inter-electrode gap is less than a certain threshold value δ_{th}^d. With increasing half-width Δ of the VDF, the position of the stability threshold δ_{th}^d shifts toward larger diode lengths, and the dependence $\delta_{th}^d(\Delta)$ is close to a linear function at a small Δ. The nonlinear stage of instability development ends with nonlinear oscillations in the vicinity of the d_0 branch. The process of instability development for solutions corresponding to branches without particle reflection can (under certain conditions) terminate by the same oscillations.

Studying the discovered nonlinear oscillations has shown that for the studied diode lengths oscillation amplitude grows with increasing in δ, and in the vicinity of the threshold, the increasing law turns out to be close to the dependence $(\delta - \delta_{th}^d)^{1/2}$, i.e., the Hopf bifurcation takes place. The calculations of nonlinear oscillations have shown that the phase plane for charged particles of both types has a rather complex configuration and demonstrates the appearance of both long-lived electrons and positrons, i.e., particles that oscillate in the vicinity
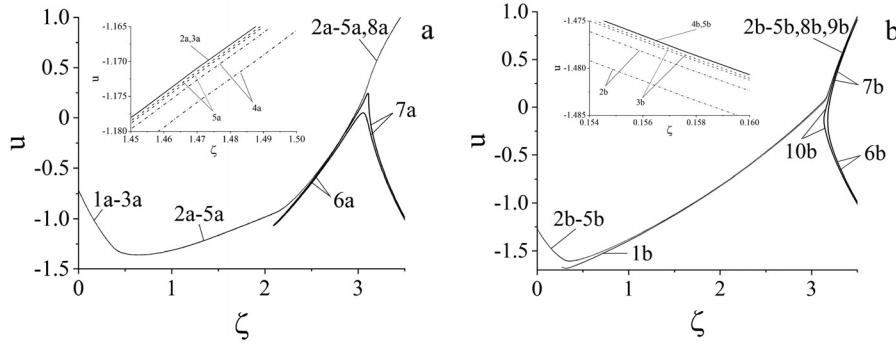
FIG. 10. The boundaries of the velocity intervals in which the positron VDF is non-zero, at the upper (a) and lower (b) points of the cycle shown in Fig. 8(b); $\delta = 3.5$, $\Delta = 0.01$. In insets, interval structure is scaled-up at $\zeta \approx 1.48$ (a) and $\zeta \approx 0.157$ (b). Note that the curve numbers on panels (a) and (b) designate different intervals.

TABLE VI. The boundaries of the velocity intervals in which the positron VDF is non-zero (u_{min} and u_{max}), at the bottom point of the cycle in the diode cross section $\zeta = 0.42$ at $\delta = 3.5$, $\Delta = 0.01$.

n	u_{min}	u_{max}	$u_{max} - u_{min}$
1b	−1.653 819 8	−1.649 713 1	0.004 106 711 9
2b	−1.600 249 4	−1.597 954 6	0.002 294 804 7
3b	−1.597 048 1	−1.596 887 6	0.000 160 494 1
4b	−1.596 670 0	−1.596 649 5	0.000 020 542 3
5b	−1.596 641 5	−1.596 640 4	0.000 001 120 4

TABLE VII. The boundaries of the velocity intervals within which the positron VDF is non-zero (u_{min} and u_{max}), at the bottom point of the cycle in the diode cross section $\zeta = 3.22$ at $\delta = 3.5$, $\Delta = 0.01$.

n	u_{min}	u_{max}	$u_{max} - u_{min}$
6b	−0.462 520 86	−0.407 972 07	0.054 548 798
7b	0.163 014 80	0.221 614 12	0.058 599 325
8b	0.256 868 25	0.266 720 51	0.009 852 254
9b	0.270 251 44	0.270 606 68	0.000 355 231
2b	0.271 069 52	0.271 114 51	0.000 044 993
3b	0.271 133 33	0.271 135 76	0.000 002 426
4b	0.271 139 06	0.271 139 54	0.000 000 474

of their VEs during several oscillation periods until they fly out onto an electrode. In the literature on studying processes in electron–positron plasma, we have not found any mention of the long-lived particles.

To date, an analytical theory of diode stability has not been created for the regime with charged particle reflection from potential extrema. Therefore, during our research, we used two numerical codes: EK-code and PIC-code. Both codes made it possible to determine the main eigenmodes from the calculations, i.e., modes that have the largest growth rate in instability case and the smallest (in absolute value) dumping factor in dumping one. The growth rates obtained by both codes have completely coincided with each other. Thus, we have demonstrated the validation of the results obtained.

In further studies of electron–positron plasma diodes, we intend to consider the relativistic regime. It should more adequately describe, for example, the behavior of plasma in a pulsar diode.[2] Although the main features of the processes in a diode are well described by the non-relativistic mode considered.

AUTHOR DECLARATIONS
Conflict of Interest

The authors have no conflicts to disclose.

Author Contributions

L. A. Bakaleinikov: Formal analysis (equal); Investigation (equal); Methodology (equal); Supervision (equal); Writing – original draft (equal); Writing – review & editing (equal). **V. I. Kuznetsov:** Conceptualization (lead); Formal analysis (lead); Investigation (equal); Methodology (lead); Project administration (lead); Supervision (lead); Validation (equal); Writing – original draft (equal); Writing – review & editing (equal). **E. Yu. Flegontova:** Formal analysis (equal); Investigation (equal); Methodology (equal); Software (equal); Supervision (equal); Validation (equal); Visualization (equal); Writing – original draft (equal); Writing – review & editing (equal). **D. P. Barsukov:** Formal analysis (equal); Investigation (equal); Methodology (equal); Software (equal); Validation (equal); Visualization (equal); Writing – original draft (equal); Writing – review & editing (equal). **I. K. Morozov:** Investigation (supporting); Software (supporting); Visualization (supporting); Writing – original draft (supporting); Writing – review & editing (supporting).

DATA AVAILABILITY

The data that support the findings of this study are available from the corresponding author upon reasonable request.

REFERENCES

[1] H. Chen and F. Fiuza, Phys. Plasmas **30**(2), 020601 (2023).
[2] V. S. Beskin, Phys. Usp. **61**(4), 353 (2018).
[3] V. I. Kuznetsov, L. A. Bakaleinikov, and E. Flegontova, Phys. Plasmas **29**(11), 112115 (2022).
[4] A. Ender, V. I. Kuznetsov, H. Schamel, and P. V. Akimov, Phys. Plasmas **11**(6), 3212 (2004).
[5] K. Qu, S. Meuren, and N. J. Fisch, Phys. Plasmas **29**, 042117 (2022).
[6] A. Ender, V. I. Kuznetsov, and A. A. Gruzdev, Plasma Phys. Rep. **42**(10), 936 (2016).

16 October 2024 11:49:50

[7] L. A. Bakaleinikov, V. I. Kuznetsov, E. Flegontova, D. P. Barsukov, and I. K. Morozov, Phys. Plasmas **30**(12), 122107 (2023).

[8] V. I. Kuznetsov and A. Ender, Plasma Phys. Rep. **36**(3), 226 (2010).

[9] R. W. Hockney and J. W. Eastwood, *Computer Simulation Using Particles* (Taylor and Francis Group, New York, London, 1988).

[10] V. I. Kuznetsov, E. Flegontova, and L. A. Bakaleinikov, Phys. Plasmas **27**(9), 092304 (2020).

[11] L. A. Bakaleinikov, V. I. Kuznetsov, and E. Flegontova, Phys. Plasmas **28**(2), 022305 (2021).

[12] J. R. Pierce, J. Appl. Phys. **15**(10), 721 (1944).